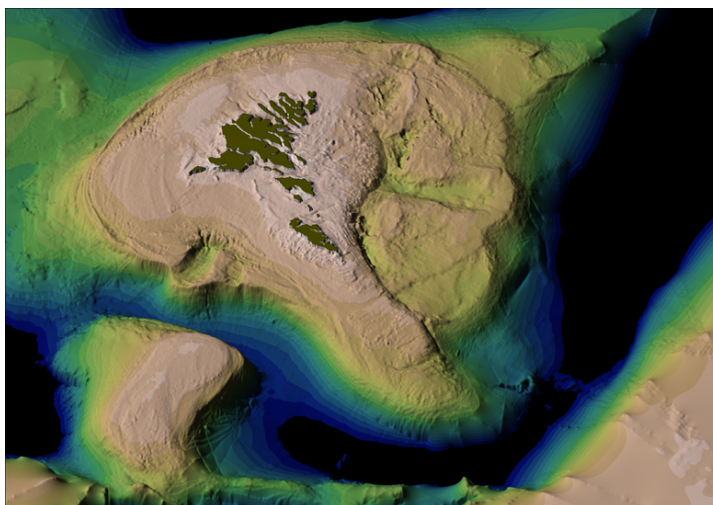


Faroe Bank Channel overflow 1995 - 2015

Tórshavn · July 2015



Bogi Hansen
Karin M. H. Larsen
Regin Kristiansen
Ebba Mortensen
Svein Østerhus

The bottom map on the cover was generated by Knud Simonsen

Abstract

This report documents measurements from moored ADCPs at four different sites across the Faroe Bank Channel from November 1995 to May 2015. Simultaneous measurements from two ADCPs deployed very close to one another suggest high data quality. The strong bottom-near currents at three of the mooring sites induce instrument tilts that frequently exceed recommended limits, but analysis of potential effects indicates that the error in volume transport associated with this is negligible. Based on the updated dataset, previously developed algorithms for overflow volume transport are slightly modified and a new time series generated. The difference from previously reported series is small.

1 Introduction

Although narrow, the Faroe Bank Channel is a significant contributor to deep water renewal of the World Ocean. With a sill depth of 840m, this channel (Figure 1.1) is the deepest passage across the Greenland-Scotland Ridge and through it there is a continuous flow of cold water, termed Faroe Bank Channel overflow (FBC-overflow). On average, the FBC-overflow is around 2 Sv, which includes the densest water crossing the ridge, although later entrainment makes the FBC-overflow less dense than the overflow through the Denmark Strait when they meet.

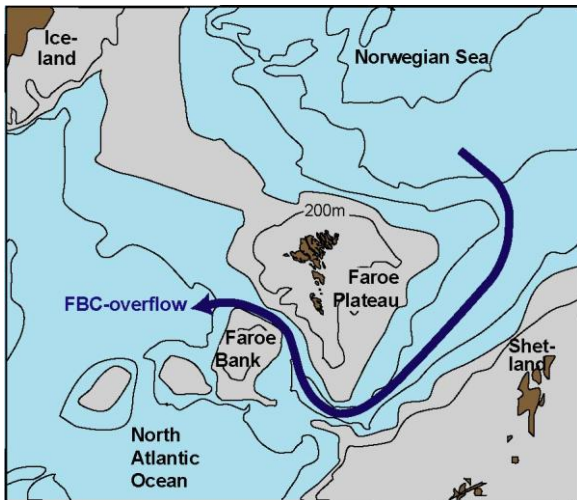


Figure 1.1 Map of the region between Iceland and Shetland. Grey areas are shallower than 500m. The Faroe Bank Channel is the narrow channel between Faroe Bank and Faroe Plateau. The blue arrow indicates the path of the Faroe Bank Channel overflow.

The FBC-overflow is therefore an important component of the climate system and, since 1995, the Faroe Marine Research Institute has monitored it in cooperation with research institutes from other nations. This has been done with quasicontinuous monitoring of the velocity field with moored ADCPs (Acoustic Doppler Current Profilers), with regular CTD cruises, and with short-term dedicated mooring experiments.

Based on an analysis of the first ten years of observations, Hansen and Østerhus (2007) discussed the main characteristics of the FBC-overflow and reported time series of the "kinematic overflow transport", determined from the velocity field, solely. Here, we extend this analysis to the whole observational period from 13 Nov 1995 to 23 May 2015 based on the same methodology, but with two modifications.

The first of these modifications is a slightly revised algorithm for calculating daily averaged velocity taking into account the tidal component. The second modification involves slightly modified algorithms for horizontal interpolation of the velocity between ADCP mooring sites and extrapolation on both sides of the channel. This was based on the whole dataset, which includes a year-long record from a new ADCP site on the northeastern flank of the channel.

In this report, we describe the ADCP data set and some issues about data quality. Then, we describe the modified methods for transport calculation. We also compare the transport time series calculated by the old and the new methodologies, but we do not discuss the results here. Those are intended for a separate publication to be submitted to a scientific journal.

2 ADCP measurements

ADCP moorings have been deployed at four different sites along a section over the sill of the channel (Figure 2.1).

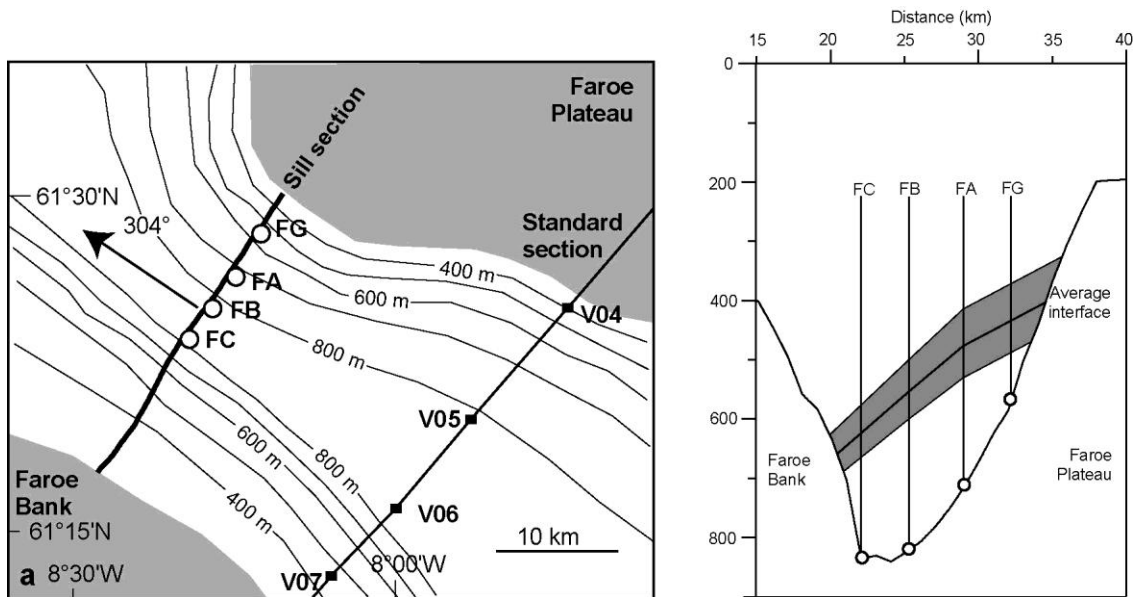


Figure 2.1 Left panel: map showing the sill section with ADCP sites indicated by circles and the standard section with standard stations indicated by black squares. Right panel: The sill section with ADCP sites indicated. The shaded area indicates a typical variation of the interface corresponding to the interface at FB varying between 500m and 600m depth.

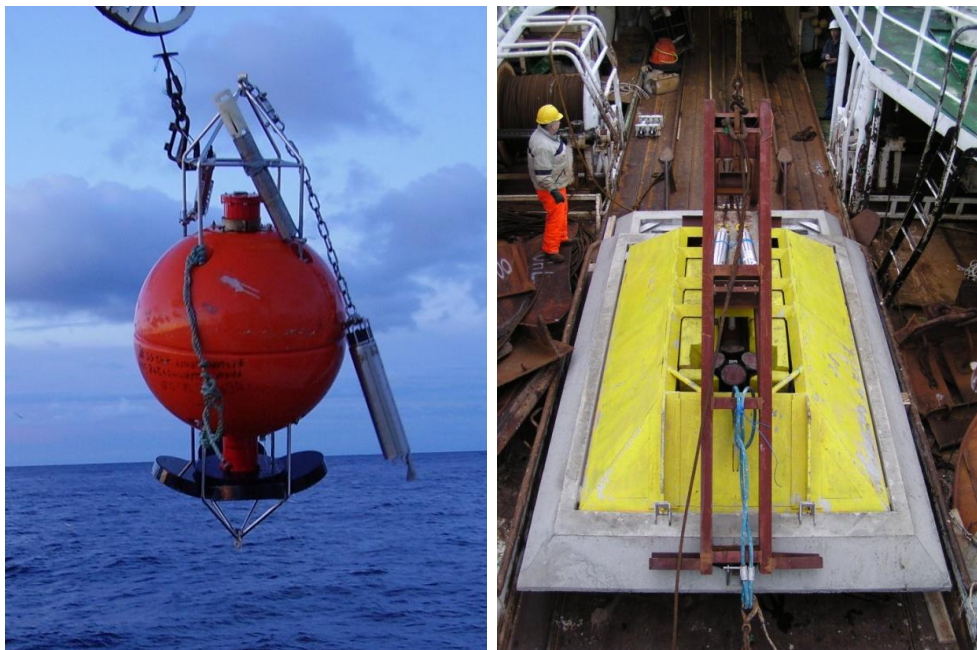


Figure 2.2 Left photo: A 75 kHz RDI Broadband ADCP in a Flotation Technology buoy with microcat and acoustic release about to be recovered in the Faroe Bank Channel. Right photo: A 150 kHz RDI Broadband ADCP in a buoyant aluminium frame (yellow), mounted on a concrete anchor, ready to be lowered to the bottom attached to a special deployment frame (brown).

A complete list of ADCP deployments is shown in Table 2.1. The dominant location is site FB, which has been occupied since Nov 1995 except for annual servicing intervals and gaps due to mooring failure. At most sites, the ADCP was located in the top of a traditional (very short) mooring (Figure 2.2, left photo), but the ADCP at site FG was located in a bottom mounted frame to protect it from fishing gear (Figure 2.2, right photo).

Table 2.1 List of ADCP deployments over the sill of the FBC. Each deployment is identified by an 8-character code including the site and the year and month of deployment. "sn" indicates serial number. Three depths are indicated: bottom depth (Bot.), instrument depth (Ins.), and center depth of the first bin (Bin1). Nbin indicates the number of bins retained after quality control and the period is specified as "yyyymmdd-yyyymmdd".

Deploymt	sn	Latitude	Longitude	Bot.	Ins.	Bin1	Nbin	Period	Days
NWFB9511	1292	61°25.051'N	08°17.207'W	813m	805m	775m	26	19951113-19960524	194
NWFB9606	1292	61°25.038'N	08°17.366'W	817m	809m	773m	26	19960616-19970524	343
NWFB9706	1292	61°24.980'N	08°16.980'W	816m	810m	774m	23	19970617-19980613	362
NWFB9807	1292	61°24.930'N	08°17.340'W	818m	812m	776m	26	19980704-19980911	70
NWFB9809	1578	61°24.950'N	08°17.130'W	815m	809m	773m	13	19980913-19990612	273
NWFB9907	1285	61°24.975'N	08°16.860'W	812m	806m	770m	25	19990705-20000618	350
NWFB0007	1642	61°24.980'N	08°16.900'W	814m	807m	771m	17	20000710-20010615	341
NWFB0107	1642	61°24.923'N	08°16.965'W	814m	808m	772m	16	20010709-20020615	342
NWFB0207	1642	61°24.942'N	08°16.870'W	812m	806m	770m	17	20020708-20030615	343
NWFB0307	1642	61°24.890'N	08°16.930'W	813m	807m	771m	17	20030706-20040611	342
NWFB0407	1642	61°24.974'N	08°16.906'W	812m	806m	770m	17	20040704-20050522	323
NWFB0506	1642	61°24.897'N	08°17.097'W	817m	811m	775m	22	20050612-20060523	346
NWFB0606	1642	61°25.051'N	08°17.244'W	812m	806m	771m	18	20060613-20070518	340
NWFB0706	1642	61°25.038'N	08°16.983'W	812m	806m	771m	17	20070610-20080515	341
NWFB0806	1642	61°25.002'N	08°16.866'W	812m	806m	771m	16	20080607-20090604	363
NWFB0906	1642	61°25.000'N	08°16.800'W	812m	806m	771m	16	20090608-20100514	341
NWFB1006	1642	61°25.000'N	08°17.000'W	814m	808m	773m	16	20100606-20110522	351
NWFB1106	1642	61°24.988'N	08°16.975'W	808m	802m	767m	16	20110613-20120521	344
NWFB1206	1642	61°25.000'N	08°16.800'W	816m	809m	774m	17	20120611-20140310	638
NWFB1306	1577	61°24.951'N	08°16.987'W	814m	807m	771m	23	20130608-20140515	342
NWFB1406	1577	61°24.951'N	08°17.000'W	809m	803m	767m	23	20140610-20150523	348
NWFA9807	1284	61°26.409'N	08°14.560'W	718m	712m	676m	23	19980704-19980911	70
NWFC9807	1285	61°23.609'N	08°18.957'W	836m	830m	794m	24	19980704-19980911	70
NWFC0207	1285	61°23.390'N	08°18.660'W	841m	835m	799m	25	20020708-20020907	62
NWFC0209	1285	61°23.680'N	08°18.700'W	826m	820m	784m	24	20020914-20030615	275
NWFC0307	1285	61°23.466'N	08°19.045'W	835m	829m	793m	25	20030706-20031031	118
NWFC0311	1285	61°23.570'N	08°18.877'W	836m	830m	794m	25	20031108-20040611	217
NWFC0407	1285	61°23.444'N	08°19.000'W	829m	823m	787m	26	20040704-20050522	323
NWFC0506	1285	61°23.365'N	08°19.094'W	815m	809m	773m	25	20050612-20060523	346
NWFC0606	1285	61°23.427'N	08°18.941'W	834m	828m	793m	26	20060613-20070518	340
NWFC0706	1285	61°23.489'N	08°18.973'W	847m	841m	806m	25	20070610-20080516	342
NWFC0806	1285	61°23.502'N	08°18.980'W	846m	840m	805m	24	20080607-20090515	343
NWFC0906	1285	61°23.550'N	08°19.010'W	841m	835m	800m	25	20090608-20100514	341
NWFC1006	1285	61°23.570'N	08°19.000'W	839m	833m	798m	23	20100606-20110522	351
NWFC1106	1285	61°23.538'N	08°19.047'W	842m	836m	801m	25	20110613-20120521	344
NWFC1306	1285	61°23.448'N	08°18.900'W	835m	828m	792m	25	20130608-20140515	342
NWFC1408	1285	61°23.100'N	08°19.100'W	818m	812m	776m	24	20140830-20150523	267
NWFG0805	3368	61°28.260'N	08°13.251'W	561m	560m	542m	51	20080517-20090515	364

3 Data quality

3.1 Comparison of two ADCPs profiling simultaneously at the same site

By a fortunate mistake, two ADCPs were deployed at the same site, site FB, and measured the overflow characteristics at this site simultaneously over a period of 276 days. The distance between the two moorings was $\approx 120\text{m}$ and the difference in bottom depth was 2m (Table 3.1), so we cannot expect identical values but the comparison almost shows that (Table 3.2), especially when we consider the transport density (Interface height \times Average velocity), which is the most important parameter for estimating overflow transport.

Table 3.1 Characteristics of two simultaneous deployments at site FB

Deploymt	sn	Latitude	Longitude	Bot.	Ins.	Bin1	Nbin	Period	Days
NWFB1206	1642	61°25.000'N	08°16.800'W	816m	809m	774m	17	20120611-20140310	638
NWFB1306	1577	61°24.951'N	08°16.987'W	814m	807m	771m	23	20130608-20140515	342

Table 3.2 Comparison between overflow characteristics measured by two ADCPs, sn 1642 and sn 1577, at site FB for 276 days from 8 June 2013 to 10 March 2014. R is correlation coefficient. α and β are the coefficients of a standard linear regression: $y = \alpha \cdot x + \beta$ where y and x are parameters for sn 1577 and sn 1642, respectively. $\Delta\alpha$ is the 95% confidence interval for α . Similarly, α_0 is the coefficient of the zero-offset linear regression: $y = \alpha_0 \cdot x$.

Parameter	Regression of sn 1577 on sn 1642				Average \pm st. error	
	R	$\alpha \pm \Delta\alpha$	β	α_0	sn 1642	sn 1577
Interface height (m):	0.995	0.986 \pm 0.011	1.3	0.991	261.4 \pm 2.1	259.2 \pm 2.1
Maximum velocity (cm s ⁻¹):	0.986	1.035 \pm 0.021	-2.4	1.013	107.7 \pm 0.6	109.1 \pm 0.6
Average velocity (cm s ⁻¹):	0.983	1.021 \pm 0.023	-0.6	1.016	96.1 \pm 0.5	97.6 \pm 0.6
Transport density (m ² s ⁻¹):	0.990	1.018 \pm 0.017	-2.7	1.007	251.2 \pm 2.3	252.9 \pm 2.4

3.2 The effect of extreme instrument tilt

With the strong bottom currents in the FBC, the mooring often will tilt more than the recommended 20° (Figure 3.1)

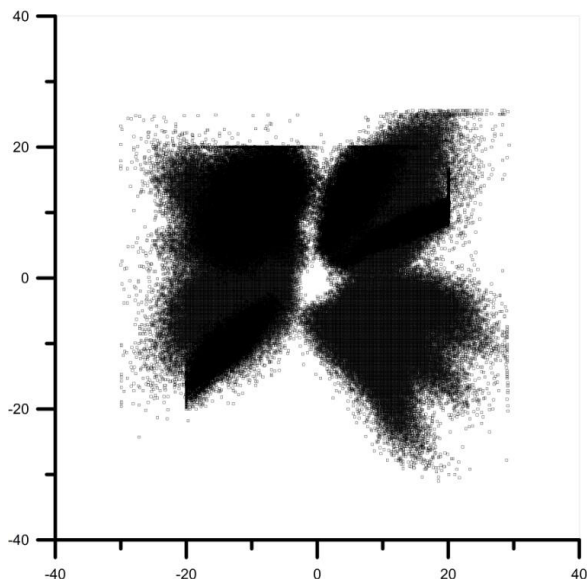


Figure 3.1 Roll plotted against pitch for all ensembles with bin 4 OK at site FB 1995 – 2014.

From pitch and roll, we can compute the instrument tilt by the formula: $\cos(\text{tilt}) = \cos(\text{pitch}) \cdot \cos(\text{roll})$. Using this, Tables 3.3 and 3.4 list ranges of pitch, roll and tilt for all deployments at sites FB and FC.

Table 3.3 Range of pitch and roll for deployments at FB.

Deplmnt	Pitch		Roll		Tilt		ADCP sn
	Min	Max	Min	Max	Min	Max	
NWFB9511	-20.00	-4.21	-20.00	-1.59	5.21	27.99	1292
NWFB9606	1.03	20.10	0.64	18.53	2.10	27.01	1292
NWFB9706	-20.00	3.05	-2.04	20.10	3.99	27.99	1292
NWFB9807	-20.00	0.71	2.64	20.08	6.66	27.56	1292
NWFB9809	-4.70	16.50	-20.00	0.40	2.59	24.85	1578
NWFB9907	-4.57	16.19	1.77	20.10	2.16	25.55	1285
NWFB0007	1.60	29.10	-27.80	3.90	1.63	39.25	1642
NWFB0107	-10.10	28.60	-2.50	25.00	1.32	37.28	1642
NWFB0207	-30.00	-0.60	-3.10	24.80	1.80	38.17	1642
NWFB0307	0.70	23.60	-31.00	-1.30	4.16	38.01	1642
NWFB0407	1.80	27.50	-25.80	3.40	3.16	34.70	1642
NWFB0506	-30.00	-1.10	-4.10	24.80	2.50	37.25	1642
NWFB0606	-30.00	-1.60	-3.10	24.70	2.73	36.82	1642
NWFB0706	-18.20	28.40	-2.90	25.10	3.31	37.13	1642
NWFB0806	-29.90	-1.80	-21.30	10.00	2.71	35.25	1642
NWFB0906	-30.00	-3.40	-15.30	12.20	3.41	32.48	1642
NWFB1006	-4.60	28.20	2.20	25.60	2.94	37.36	1642
NWFB1106	-2.30	29.40	0.80	25.60	2.25	37.88	1642
NWFB1206	-29.90	-1.00	-24.30	7.40	2.72	35.84	1642
NWFB1306	2.60	26.60	-3.40	16.70	4.00	30.64	1577
NWFB1406	-25.50	0.80	-1.30	17.80	1.64	30.43	1577

Table 3.4 Range of pitch and roll for deployments at FC.

Deplmnt	Pitch		Roll		Tilt		ADCP sn
	Min	Max	Min	Max	Min	Max	
NWFC9807	-1.50	20.04	2.11	20.09	2.11	28.01	1285
NWFC0207	-15.19	18.37	-20.00	-3.38	6.22	26.71	1285
NWFC0209	-17.83	17.56	-20.00	-1.64	2.65	26.21	1285
NWFC0307	4.62	20.20	-15.04	-1.48	7.32	24.85	1285
NWFC0311	-8.58	20.00	-20.00	-1.99	2.68	26.79	1285
NWFC0407	-20.00	-0.90	-2.30	20.02	2.06	27.99	1285
NWFC0506	-20.00	0.86	-20.00	1.67	1.46	27.19	1285
NWFC0606	-0.94	20.10	-20.00	-0.03	1.67	27.09	1285
NWFC0706	-20.00	-2.93	-4.42	20.04	4.50	27.50	1285
NWFC0806	-2.86	20.10	-20.00	4.86	4.75	26.93	1285
NWFC0906	-5.07	20.05	0.57	20.17	1.02	26.73	1285
NWFC1006	-19.00	3.76	-20.00	-2.01	2.57	25.36	1285
NWFC1106	1.71	20.17	-20.00	4.64	2.79	24.00	1285
NWFC1306	2.41	20.10	-18.61	3.88	2.92	23.93	1285
NWFC1408	-14.28	9.68	2.68	20.21	2.77	24.18	1285

Apparently, the "old" ADCPs sn 1292 and 1285 (perhaps also 1578) did not report pitch and roll values numerically higher than 20°, whereas for sn 1642 and 1577, the limit was 30° (Tables 3.3 and 3.4).

We expect the tilt to be determined by the strength of the bottom-near current and check this by plotting the speed of the deepest bin (bin 1) against tilt for all deployments at FB up to 2014 (Figure 3.2). There is a relationship but it appears quite noisy. This was not caused by different conditions during different deployments as demonstrated by plotting individual deployments separately.

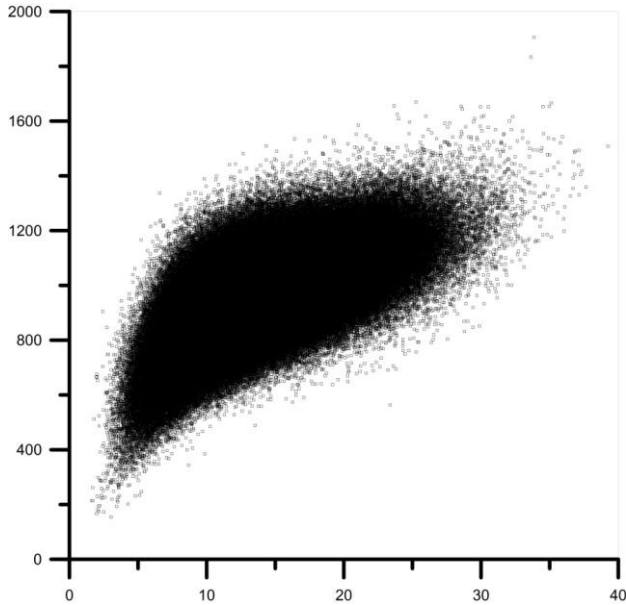


Figure 3.2 Speed of bin 1 (mm/s) plotted against tilt for all OK ensembles at site FB 1995 – 2014.

According to the manufacturer, extreme tilt may affect the operation of the compass and might therefore give erroneous current directions. To check this, we plot the current direction at bin 4, which is usually close to the core of the overflow against tilt for all ensembles at FB and FC up to 2014 (Figure 3.3). From the figure, there may be an effect for FC, but it is small and a potential error in the along-channel velocity would be less than 1%.

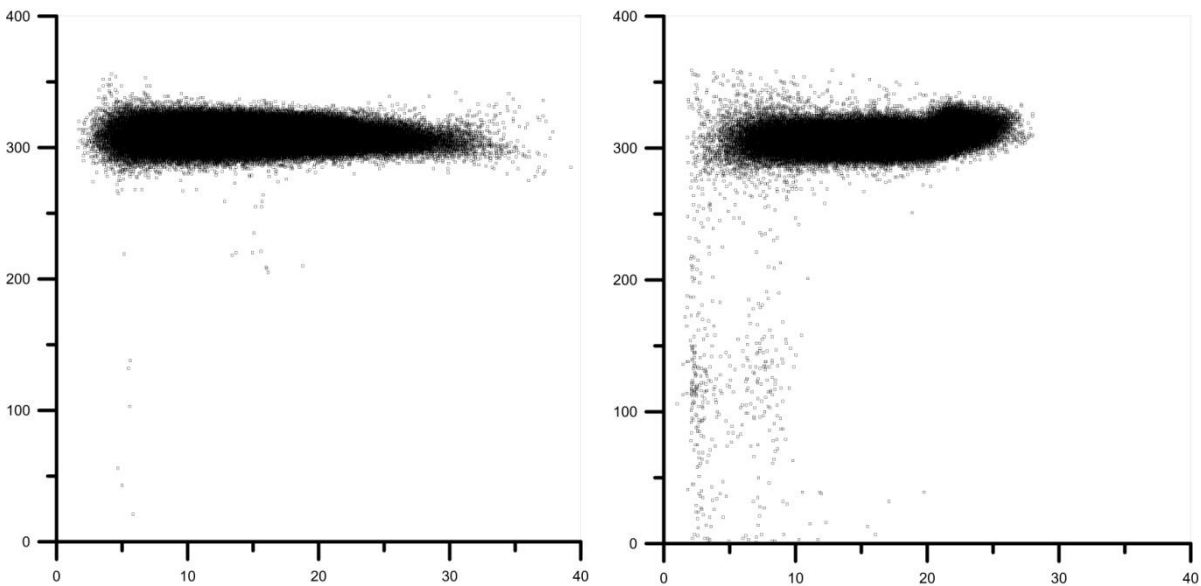


Figure 3.3 Current direction at bin 4 plotted against tilt for all OK ensembles at site FB 1995 – 2014 (left) and at FC 1998 – 2014 (right).

Another potential effect of extreme tilt could be errors in the transformation from instrument to earth coordinates. If an erroneous tilt value is used in this transformation, the total velocity should still be correct but its projection onto horizontal and vertical directions would be wrong. To check this, we therefore plot

the vertical velocity of bin 4 against tilt for individual ensembles (Figure 3.4). For both sites, the picture changes for large tilts, but especially FC looks suspicious. To explore this, we plot the ratio of vertical to horizontal velocity for bin 4 in Figure 3.5 with similar results.

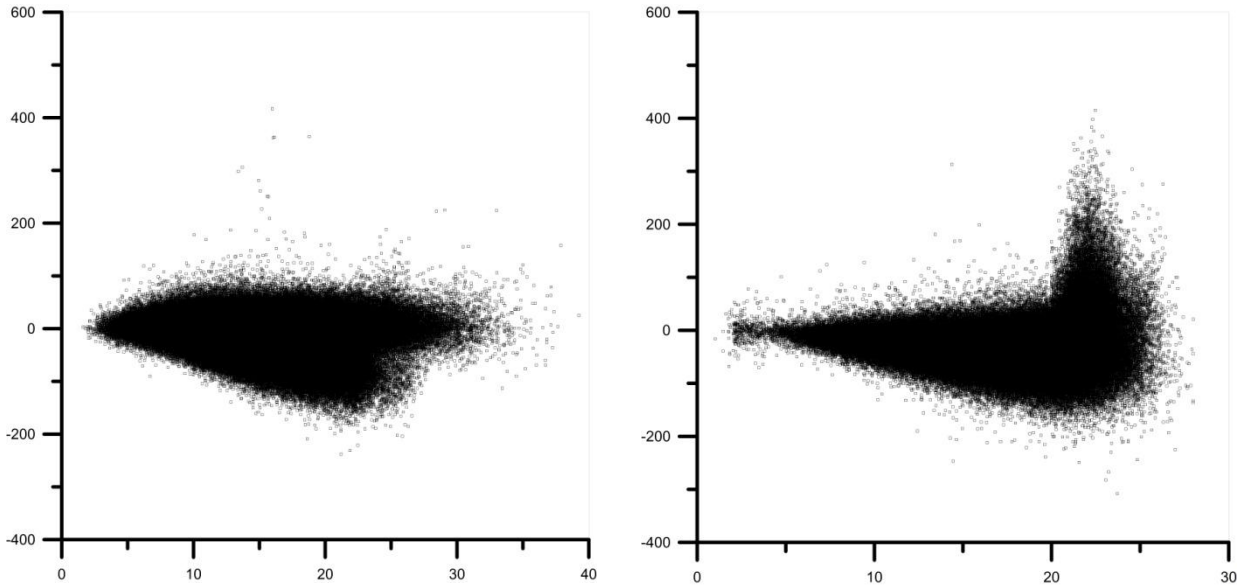


Figure 3.4 Vertical velocity of bin 4 (mm/s) plotted against tilt for all OK ensembles, for which horizontal velocity at bin 4 is > 20 cm/s for FB (left) and FC (right).

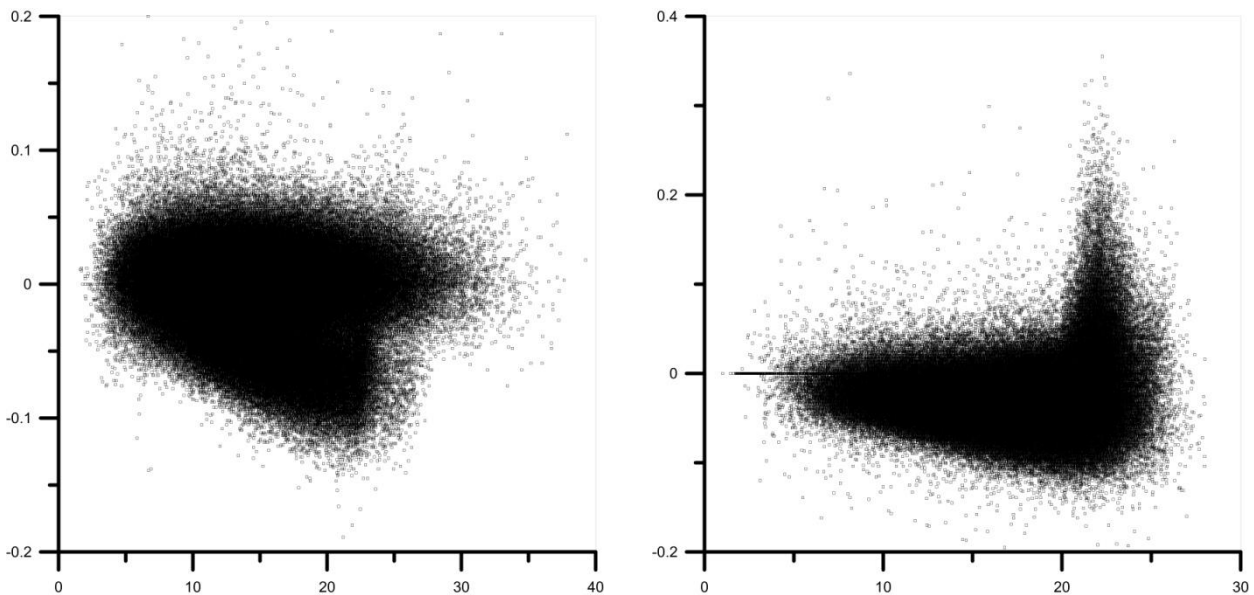


Figure 3.5 Ratio of vertical velocity to horizontal velocity of bin 4 plotted against tilt for all OK ensembles at FB (left) and FC (right). A few outliers (mainly for tilt < 20) have been clipped. For horizontal velocity < 20 cm/s, the ratio is set to 0.

Considering individual deployments, we find that the special shape for FC in Figure 3.4 appears in some deployments, but not others (Figure 3.6). Perhaps this has to do with whether it is pitch or roll that is extreme (Table 3.4).

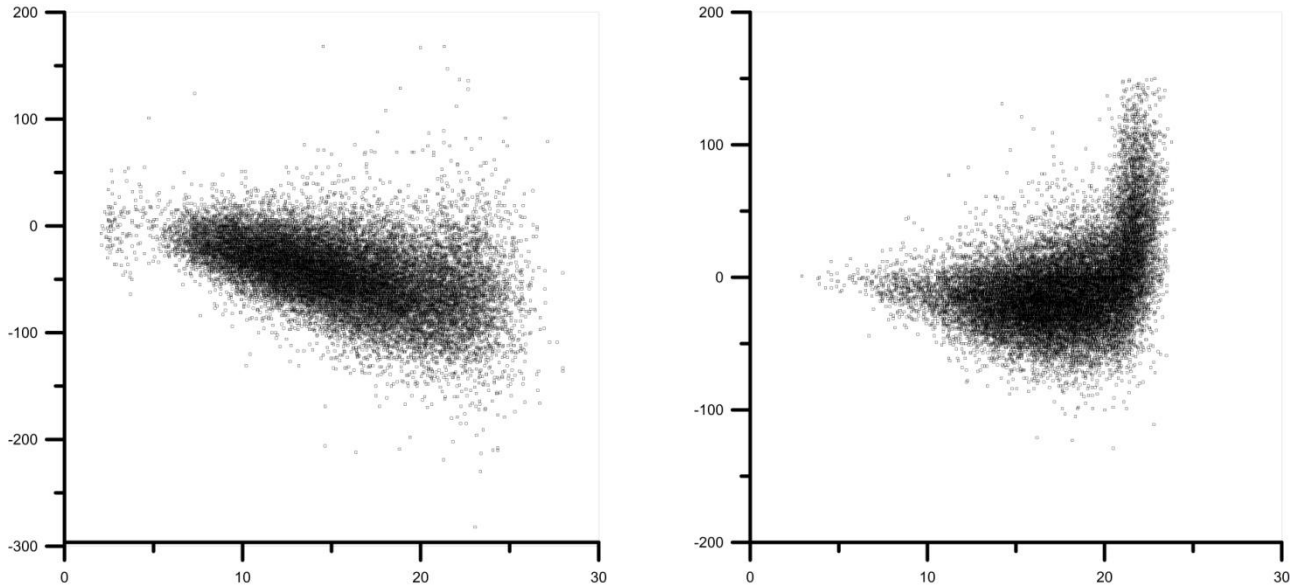


Figure 3.6 Vertical velocity plotted against tilt for deployment FC0407 (left) and FC1306 (right).

To get a more quantitative impression, the right panel in Figure 3.7 shows the average tilt of the velocity vector and its standard deviation as a function of instrument tilt for both FB and FC. Up to an instrument tilt of 20° or a little more, the velocity tilts slightly downwards with negative (downwards) vertical velocity components. This is not unexpected, since we would expect a negative vertical velocity component at the sill of an overflow channel. Whether the magnitude of the velocity tilt (1-3%) or its increase with instrument tilt are realistic, is more difficult to ascertain.

In any case, the behaviour changes when the tilt exceeds 20° and this is likely to be an error due to incorrect transformation to earth coordinates, but the velocity tilt remains fairly small. To see the effect of this error, assume that we have measured a vertical velocity component w' and a horizontal velocity component u' . Assume further that the magnitude of the three-dimensional velocity vector was correctly measured by the ADCP, but the flow in reality was horizontal: $w=0$. The correct horizontal velocity component, u , is then given by:

$$u = \sqrt{u'^2 + w'^2} = u' \cdot \sqrt{1 + \left(\frac{w'}{u'}\right)^2} \approx u' \cdot \left(1 + \frac{1}{2} \cdot \frac{w'}{u'}\right)$$

as long as the measured velocity tilt w'/u' is small. If the assumption of horizontal flow is correct, the error in average horizontal velocity will be $\lesssim 1\%$ for both FB and FC even for the most extreme instrument tilts (Figure 3.7, right panel). For FB, which is the basic site, this is valid also for all the measurements within \pm one standard deviation. As mentioned, we would expect a downward vertical velocity component but it is not immediately obvious that the velocity tilt should increase with instrument tilt (overflow speed). If that

effect is fictional then the horizontal velocity component is actually more accurate for very high instrument tilts than for those around 20°.

The left panel in Figure 3.7 shows the accumulated frequency of instrument tilt, that is the fraction of OK ensembles that exceeded specified values of instrument tilt. We see that between 10% (FB) and 20% (FC) of all OK ensembles had tilts exceeding 20°. At FB, only 1% exceeded 25° whereas less than one in thousand exceeded this tilt for FC.

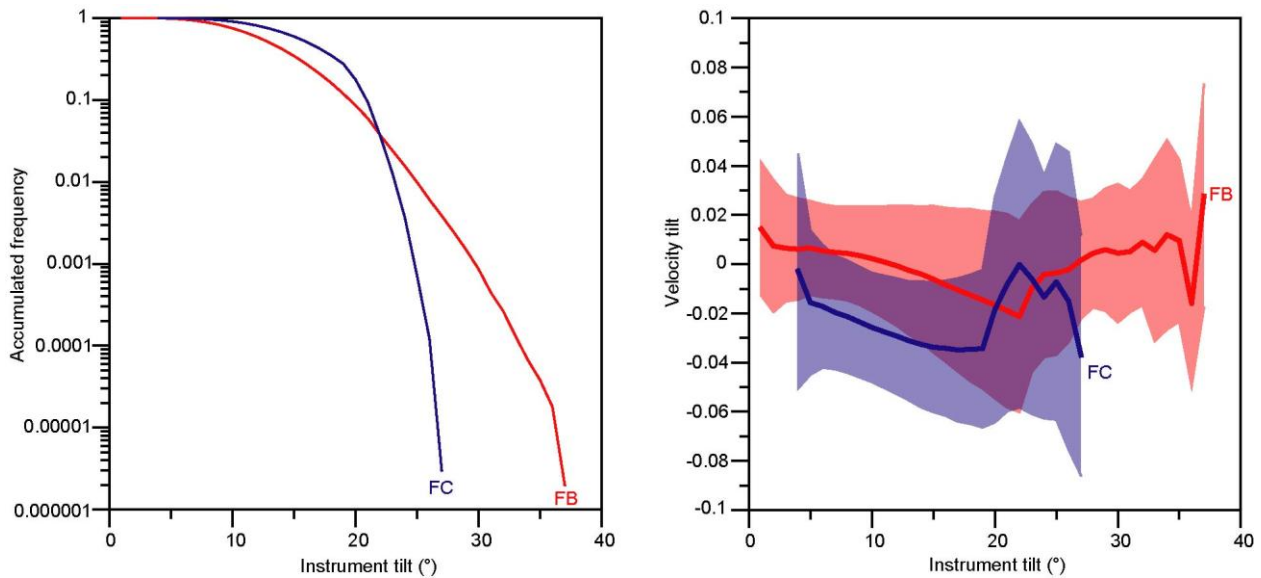


Figure 3.7 Left panel: Accumulated frequency of ensembles with instrument tilt exceeding specified values. Right panel: Velocity tilt (vertical velocity divided by average horizontal velocity) at bin 4. Thick lines indicate the average velocity tilt with semitransparent areas indicating \pm one standard deviation. Both panels are for all OK ensembles at FB (red) and FC (blue), including 2014-2015.

Summarizing, it seems clear that the extreme instrument tilts do not affect measured current direction but they do induce errors in the horizontal velocity component. It is, however, unlikely that the average velocity or overflow transport are wrong by more than 1%, especially for the measurements at site FB.

4 Overflow characteristics and transport

4.1 Characterizing the overflow layer

Following the method described by Hansen and Østerhus (2007), we characterize the overflow layer at each ADCP site by a few parameters. The overflow layer is bounded on top by the interface (Figure 4.1). The location of the interface on any given day t may be characterized by its height above bottom, $H_i(t)$, or its depth, $D_i(t)$. The deepest part of the overflow layer is the logarithmic boundary layer, which is characterized by the velocity at its top, $V_L(t)$. The vertically averaged velocity between the interface and the logarithmic boundary layer is termed the average velocity, $V_i(t)$.

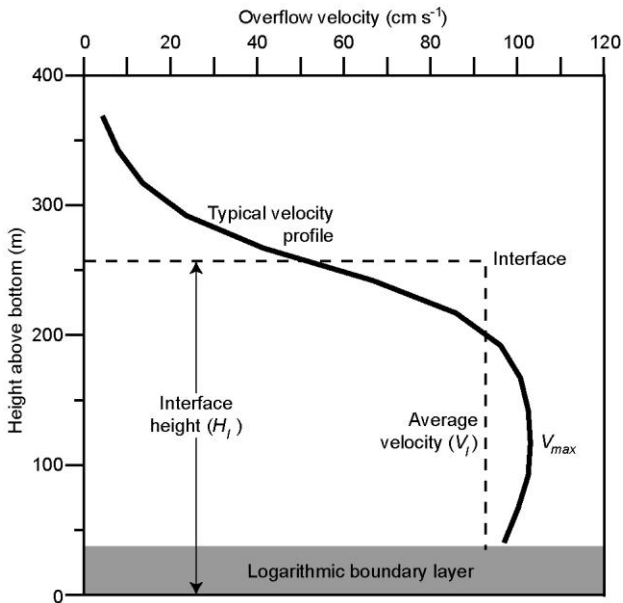


Figure 4.1 The characteristic parameters for the overflow layer at each site. For each day, the interface level is determined as the depth at which the velocity (towards 304°) is half the maximum velocity (V_{max}) on that day. The interface height is required not to exceed a maximum, which for sites FC, FB, and FA, is 400m and is exceedingly rare. For FG, the maximum interface height is set to 290m and happens more frequently.

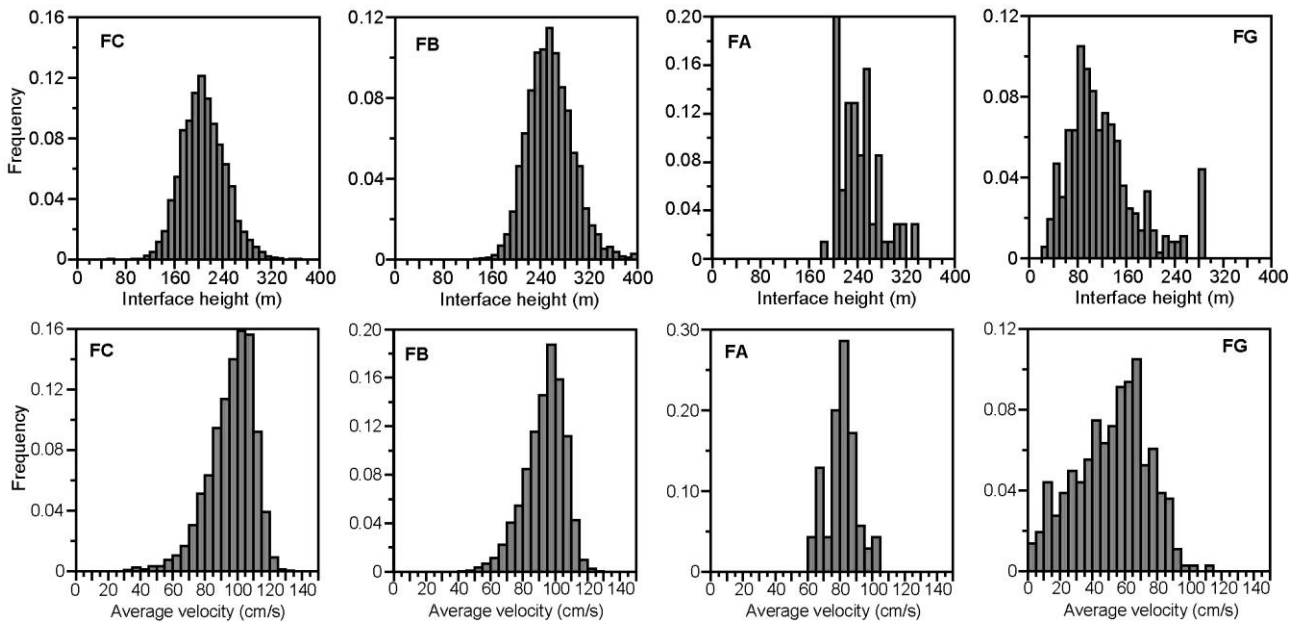


Figure 4.2 Frequency distributions (histograms) of daily mean interface height (top row) and average velocity (bottom row) for the four ADCP sites.

The distributions of interface height and average velocity for each of the four sites are shown in Figure 4.2. The characteristics at FC, FB, and FA were discussed in Hansen and Østerhus (2007) and will not be repeated here although additional data have been acquired at both FC and FB. In contrast to the other three sites, the new site, FG, is seen to have less stable overflow. Both the interface height and the average velocity may approach and even reach zero, but usually the daily mean average velocity at FG is above 40 cm/s (Figure 4.2, bottom right) indicating overflow.

Site FG is clearly close to the boundary of the overflow layer, as also indicated by the bottom temperature measured by the ADCP (Figure 4.3), which usually (78%) is below 4.5°C, but only occasionally below 2°C. We might have expected to see a clear relationship between bottom temperature and interface height and average velocity and there are indications of that. The coldest bottom water is not seen when the interface height or average velocity are low and the highest average velocities are associated with cold bottom water (Figure 4.3). The relationships are, however, quite noisy; especially for interface height, which may be quite high for all bottom temperatures (Figure 4.3, middle panel). This may perhaps be related to convective events close to site FG (Hansen et al., in prep.)

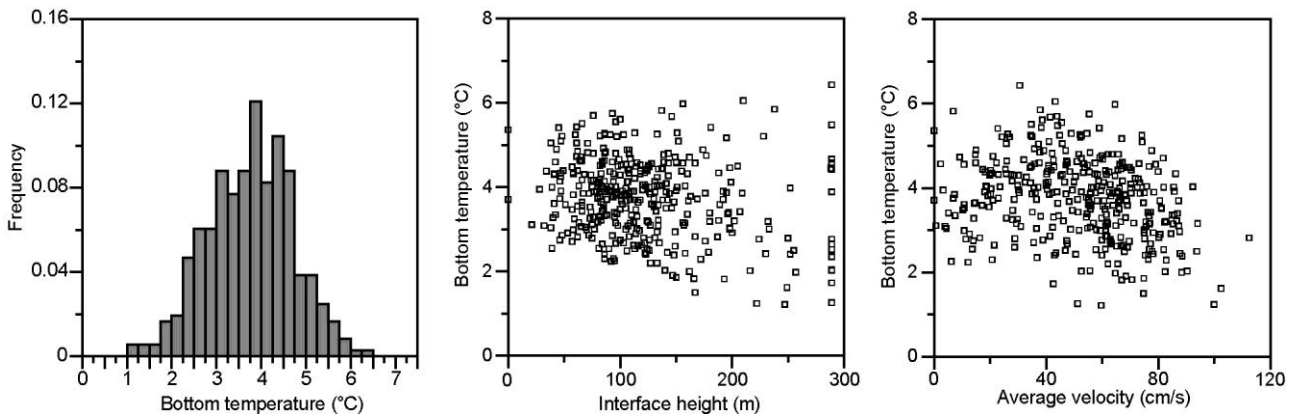


Figure 4.3 Bottom temperature at site FG. Left panel: Frequency distribution (histogram) of daily mean bottom temperature. Middle panel: daily mean bottom temperature plotted against interface height. Right panel: daily mean bottom temperature plotted against average velocity.

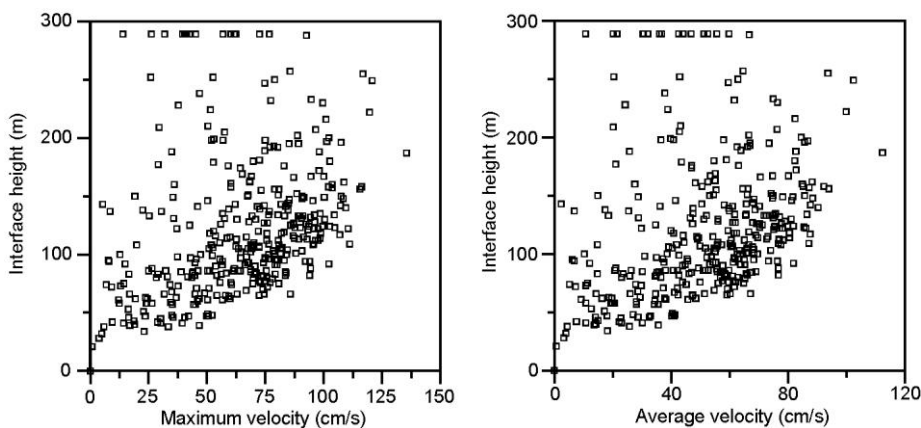


Figure 4.4 Daily mean interface height at FG plotted against maximum velocity on the profile (left panel) and against the average velocity (right panel).

A somewhat similar picture is seen when we plot interface height against the maximum or average velocity at FG (Figure 4.4). When the velocities are high, the interface height is also relatively high. However, high interfaces may also occur for low velocities.

Hansen and Østerhus (2007) found a fairly high coherence in overflow parameters across the channel from site FC to FA. This is confirmed with the updated dataset and may partly be extended to include site FG (Table 4.1). This table shows correlation and regression coefficients for the relationship for four different parameters between site FB and the other sites. For all parameters and all sites, we find correlation coefficients exceeding 0.8, except for interface depth (and interface height) at site FG. If we only include days with bottom temperatures below 4.5°C at FG, the relationship is considerably clearer (Table 4.1d), but still not very impressive.

Table 4.1 Comparison of daily mean overflow parameters between site FB and one of the other sites for all days with simultaneous measurements at both (Table 2.1). N is the number of values. R is the correlation coefficient. $\alpha \pm \Delta\alpha$ and β are the regression coefficients in the regression: $FX = (\alpha \pm \Delta\alpha) \cdot FB + \beta$, where $\Delta\alpha$ is the 95% confidence interval for α . R_0^2 and α_0 are for the zero-offset regression: $FX = \alpha_0 \cdot FB$. Here, FX is one of the sites FC, FA, or FG. Averages and β are in m for interface depth and in m/s for the velocities. For site FG, Table 4.1c includes all the measurements, whereas Table 4.1d only includes data with bottom temperature < 4.5°C.

Table 4.1a: FC regressed on FB. Average distance: 3306m

Parameter	N	Standard regression				Zero-offset		Averages	
		R	α	$\Delta\alpha$	β	R_0^2	α_0	FB	FC
Interface depth D_I :	4080	0.923	0.880	0.011	138	1.000	1.129	553.7	625.6
Velocity bin 1:	4080	0.906	1.125	0.016	-0.074	0.998	1.049	0.955	1.000
Maximum velocity:	4080	0.893	1.019	0.016	0.006	0.998	1.025	1.058	1.084
Average velocity V_I :	4080	0.878	1.010	0.017	0.011	0.998	1.021	0.942	0.962

Table 4.1b: FA regressed on FB. Distance 3699m

Parameter	N	Standard regression				Zero-offset		Averages	
		R	α	$\Delta\alpha$	β	R_0^2	α_0	FB	FA
Interface depth D_I :	70	0.858	1.162	0.169	-167	0.999	0.860	552.1	474.3
Velocity bin 1:	70	0.814	1.018	0.176	-0.145	0.998	0.873	0.989	0.863
Maximum velocity:	70	0.829	0.935	0.152	-0.082	0.998	0.860	1.091	0.938
Average velocity V_I :	70	0.831	0.940	0.153	-0.103	0.998	0.835	0.973	0.812

Table 4.1c: FG regressed on FB for all bottom temperatures. Distance FB - FG: 6854m

Parameter	N	Standard regression				Zero-offset		Averages	
		R	α	$\Delta\alpha$	β	R_0^2	α_0	FB	FG
Interface depth D_I :	343	0.557	0.977	0.156	-109	0.994	0.784	563.4	441.4
Velocity bin 1:	343	0.878	1.803	0.105	-1.085	0.953	0.632	0.911	0.557
Maximum velocity:	343	0.822	1.585	0.118	-0.974	0.954	0.637	1.008	0.624
Average velocity V_I :	343	0.842	1.496	0.103	-0.842	0.953	0.576	0.898	0.501

Table 4.1d: FG regressed on FB for bottom temperature < 4.5°C. Distance FB - FG: 6854m

Parameter	N	Standard regression				Zero-offset		Averages	
		R	α	$\Delta\alpha$	β	R_0^2	α_0	FB	FG
Interface depth D_I :	268	0.626	1.057	0.160	-150	0.994	0.790	559.2	441.0
Velocity bin 1:	268	0.903	1.848	0.107	-1.113	0.956	0.652	0.914	0.576
Maximum velocity:	268	0.857	1.655	0.121	-1.024	0.957	0.662	1.010	0.648
Average velocity V_I :	268	0.873	1.548	0.105	-0.876	0.956	0.597	0.903	0.522

In a standard regression analysis: $y_i = \alpha \cdot x_i + \beta$, the offset, β , is fitted to give minimum least square error. This is reasonable for interface depth, but if there is a linear relation between the velocities at two sites then both should be zero at the same time, which implies zero offset. In addition to the standard regression analyses, Table 4.1 therefore shows results from regression analyses requiring zero offset: $y_i = \alpha_0 \cdot x_i$. The parameter R_0^2 is an indicator of the quality of this fit. It is defined as:

$$R_0^2 = \frac{\left(\sum x_i \cdot y_i\right)^2}{\sum x_i^2 \cdot \sum y_i^2}$$

The reason for the low correlation coefficient between interface depth (or height) at FG and FB is illustrated in Figure 4.5. For many days, there is a fairly tight relationship between the two parameters, especially if we only include days with bottom temperature less than 4.5°C (Figure 4.5, right panel), but then there are some days when the interface at FG is much higher than indicated by this relationship. Again, we may hypothesize that they are associated with convective events (Hansen et al., in prep.).

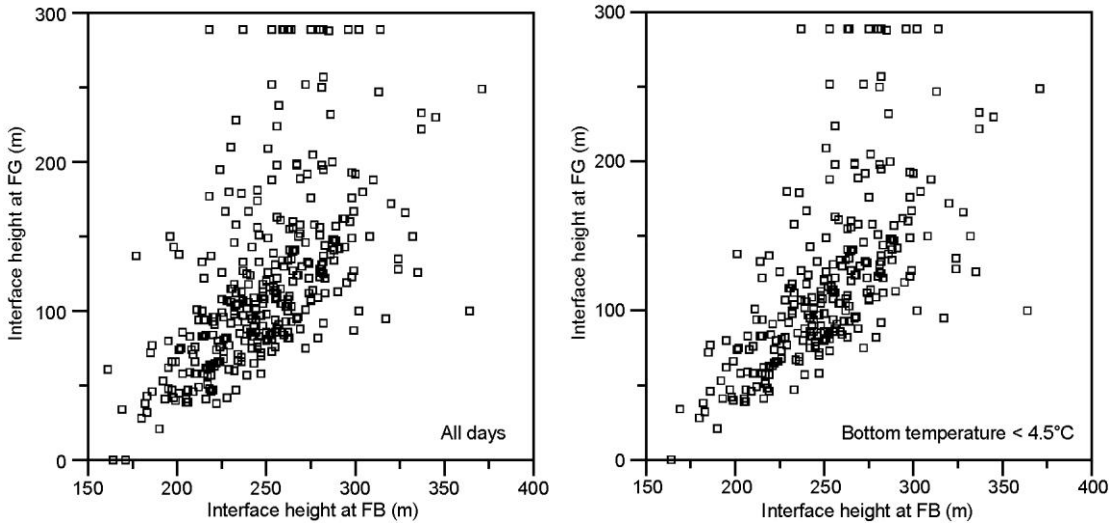


Figure 4.5 Daily averaged interface height at FG plotted against interface height at FB for all days with measurements (left panel) and for only days with bottom temperature less than 4.5°C

4.2 Calculation of overflow volume transport

Following Hansen and Østerhus (2007), we calculate the "kinematic overflow transport" defined as the volume transport below the interface (Figure 4.1), and use the equation:

$$Q(t) = \int_{x_1}^{x_2} v_I(x,t) \cdot (b(x) - d_I(x,t) - h_L) dx + \int_{x_1}^{x_2} q_L(x,t) dx \quad (1)$$

For the whole period, we only know the characteristics of the overflow layer at site FB: interface depth $D_{IB}(t)$, average velocity $V_{IB}(t)$, and the velocity of bin 1, $v_{LB}(t)$, which is used to characterize the velocity at the top of the logarithmic layer. At all other locations along the sill section, we assume linear variation. West of and at site FA, we use the equations:

$$d_I(x,t) = D_0 - \alpha \cdot (x - x_B) + [1 + \beta \cdot (x - x_B)] \cdot (D_{IB}(t) - D_0) \quad (2)$$

$$v_I(x,t) = [1 - \gamma \cdot (x - x_B)] \cdot V_{IB}(t) \quad (3)$$

$$v_L(x,t) = [1 - \lambda \cdot (x - x_B)] \cdot V_{LB}(t) \quad (4)$$

to calculate the depth of the interface, $d_I(x,t)$ (in m), the average velocity (toward 304°), $v_I(x,t)$ (in m/s), and the velocity, $v_L(x,t)$ (in m/s), at the top of the logarithmic layer at horizontal location x and time t . The horizontal coordinate x is the distance (in m) from the 100m depth contour on the Faroe Bank, following the section (Figure 2.1, right panel). The coefficients are listed in the top two rows in Table 4.2, where the first line is used for the region west of FB and based on Table 4.1a, whereas the second row is used between FB and FA, based on Table 4.1b.

Table 4.2 Coefficients used in Eqs (2) to (4) (top two rows) and in Eqs. (5) to (7)

	D_0	α	β	γ	λ
West of FB:	553.7	0.0217	$3.63 \cdot 10^{-5}$	$6.40 \cdot 10^{-6}$	$1.48 \cdot 10^{-5}$
Between FB and FA:	552.1	0.0210	$4.38 \cdot 10^{-5}$	$4.46 \cdot 10^{-5}$	$3.43 \cdot 10^{-5}$
East of FA:		0.0132	$2.71 \cdot 10^{-4}$	$2.78 \cdot 10^{-4}$	

East of site FA, we use Eqs. (5) to (7) with the coefficients in the bottom row of Table 4.2, based on Table 4.1d.

$$d_I(x,t) = d(x_A,t) - \alpha \cdot (x - x_A) \quad (5)$$

$$v_I(x,t) = v_I(x_A,t) \cdot [1 + \beta \cdot (x - x_A)] - \gamma \cdot (x - x_A) \quad (6)$$

$$v_L(x,t) = v_I(x,t) \quad (7)$$

Using these equations, we have calculated the kinematic overflow transport for all days with ADCP measurements at site FB. In Figure 4.6, these values are compared to the old estimates that were based on the old algorithms for daily averaging and horizontal interpolation. The good correspondence indicated in this figure is verified in Table 4.3.

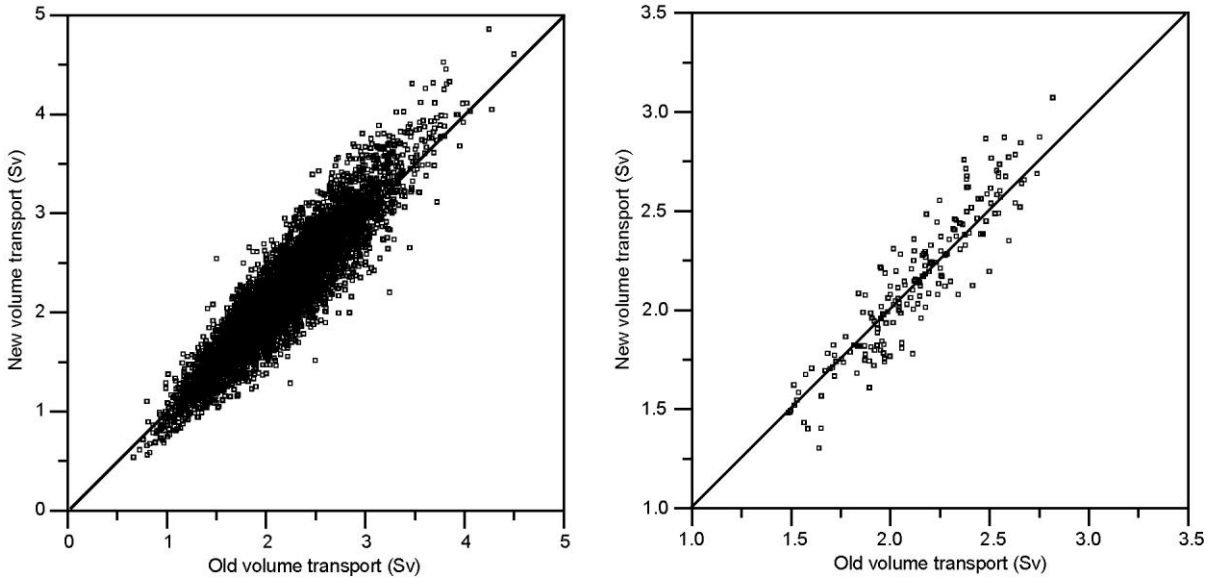


Figure 4.6 The new estimate of kinematic volume transport of FBC-overflow plotted against the old estimate calculated by the Hansen and Østerhus (2007) algorithm and using the old ADCP data from 13 Nov 1995 to 15 May 2014. Left panel: daily values. Right panel: monthly values for months with at least 28 days.

Table 4.3 Comparison of the old and the new volume transport series for daily and monthly averaged data from 13 Nov 1995 to 15 May 2014. N is the number of values. R is the correlation coefficient. $\alpha \pm \Delta\alpha$ and β are the regression coefficients in the regression: $\text{New} = (\alpha \pm \Delta\alpha) \cdot \text{Old} + \beta$, where $\Delta\alpha$ is the 95% confidence interval for α . R_0^2 and α_0 are for the zero-offset regression: $\text{New} = \alpha_0 \cdot \text{Old}$. Averages and β are in Sv.

	N	Standard regression				Zero-offset		Averages	
		R	α	$\Delta\alpha$	β	R_0^2	α_0	Old	New
Daily:	6413	0.926	1.059	0.011	-0.10	0.995	1.014	2.15	2.18
Monthly:	190	0.922	1.096	0.067	-0.19	0.998	1.011	2.13	2.15

As a further check, we have used Eqs. (2) to (7) to simulate interface height, average velocity, and velocity of bin 1 at sites FC, FA, and FG for all days with ADCP data at FB and compared these values to those measured at the sites with reasonable agreement (Figure 4.7).

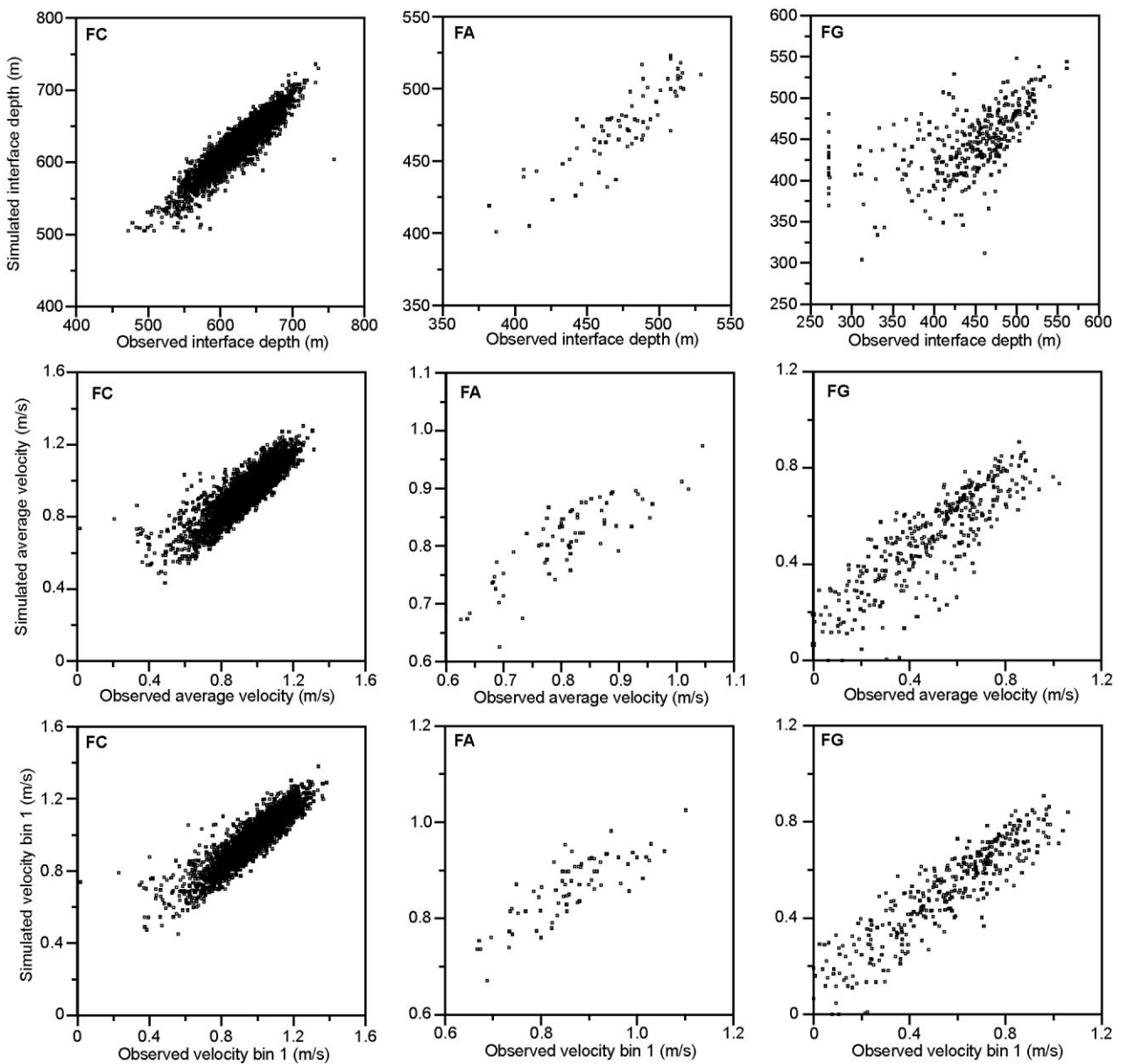


Figure 4.7 Overflow parameters at sites FC, FA, and FG simulated by Eqs. (2) to (7) from measurements at FB plotted against measured values at the sites.

References

Hansen, B. and Østerhus, S.: Faroe Bank Channel overflow 1995-2005, *Prog. Oceanogr.*, 75, 4, 817-856, doi:10.1016/j.pocean.2007.09.004, 2007.

